

Polarized confocal theta microscopy

Olivier Haeberlé^{a*}, Hiromitsu Furukawa^b, Koji Tenjimbayashi^b

^a Groupe LabEl – Laboratoire MIPS, Université de Haute-Alsace IUT Mulhouse, 61, rue A. Camus, 68093 Mulhouse cedex, France

^b OptMec, Photonics Research Institute, AIST, Namiki 1-2, Tsukuba, Ibaraki 305-8564, Japan

Received 15 July 2002; accepted 6 September 2002

Note presented by Ionel Solomon.

Abstract

We propose a comprehensive treatment of theta microscopy based on dipole emission, which better describes fluorescence emission than the isotropic emission model, as fluorescence emission is often polarized. Formulas describing the point spread function for polarized confocal fluorescence theta microscopy are given. Examples are given and some advantages of polarized theta fluorescence microscopy are presented. *To cite this article:* O. Haeberlé et al., C. R. Physique 3 (2002) 1445–1450.

© 2002 Académie des sciences/Éditions scientifiques et médicales Elsevier SAS

fluorescence microscopy / reflection microscopy / theta microscopy

Microscopie confocale theta polarisée

Résumé

Nous présentons un modèle pour la microscopie de fluorescence theta basé sur le rayonnement dipolaire, qui décrit mieux le phénomène de fluorescence que le modèle isotropique, car l'émission de fluorescence est souvent polarisée. Les formules décrivant la tache de diffraction pour la microscopie de fluorescence polarisée en montage theta sont données. Des exemples sont donnés, et certains avantages à utiliser la polarisation en microscopie de fluorescence theta sont présentés. *Pour citer cet article :* O. Haeberlé et al., C. R. Physique 3 (2002) 1445–1450.

© 2002 Académie des sciences/Éditions scientifiques et médicales Elsevier SAS

microscopie de fluorescence / microscopie en réflexion / microscopie theta

Version française abrégée

En microscopie classique et confocale [1,2], un compromis entre résolution et distance de travail doit être accepté, les objectifs à grande distance de travail ayant une faible ouverture numérique, et donc une faible résolution. Le microscope theta a été proposé pour pallier à cet inconvénient. Il consiste à utiliser deux objectifs de microscope pour l'excitation et la détection, dont les axes optiques sont perpendiculaires [3]. La Fig. 1 en décrit le principe. L'objectif 1 est utilisé pour illuminer le specimen, et la détection se fait au travers de l'objectif 2.

Nous proposons un traitement détaillé du microscope theta, basé sur la théorie vectorielle de la diffraction pour les objectifs à grande ouverture numérique, et sur le modèle d'émission dipolaire.

* Correspondence and reprints.

E-mail address: o.haeberle@uha.fr (O. Haeberlé).

La configuration du microscope theta oblige à utiliser des objectifs sans lamelle, la RIO d'excitation est donc calculée à l'aide du modèle de Richards et Wolf [1]. Les équations (1), (2) donnent le champ électromagnétique au point focal. La RIO du microscope theta est alors souvent calculée à l'aide de l'équation (3), en considérant une émission de fluorescence isotrope et non-polarisée [3]. L'émission de fluorescence étant polarisée [4,5], il est plus rigoureux de considérer le champ émis par un dipole [6,7]. Le moment et le champ dipolaires sont alors donnés par les équations (4) et (5). Le champ est capté par l'objectif 2, et refocalisé sur le détecteur. Avec un objectif de refocalisation de faible ouverture numérique, le détecteur quadratique enregistre alors le carré de la transformée de Fourier du champ électromagnétique : équation (7), les équations (6a) et (6b) décrivant le champ, calculé à l'aide des intégrales (8). La formule (9) lie les angles entre l'objectif de détection 2 et la lentille de refocalisation [6,7].

Nous avons calculés les RIO pour un microscope theta utilisant des objectifs d'ouverture numérique N.A. = 0,8 à immersion à eau [8], avec une excitation à $\lambda = 400$ nm et une détection $\lambda = 450$ nm (Cascade Blue from Molecular Probes). La Fig. 2 montre les résultats obtenus. La Fig. 2(a) montre la RIO calculée avec le modèle isotrope. Les Figs. 2(b) et 2(c) montrent la RIO calculée avec le modèle dipolaire, pour une excitation x -polarisée et une détection x -polarisée et pour une excitation z -polarisée et une détection x -polarisée, respectivement. Le modèle isotrope a tendance à surestimer la résolution en x , et sous-estimer la résolution en z et en y . La Fig. 3 montre les RIO pour une détection y -polarisée. Non seulement les formes des RIO sont très différentes, mais surtout l'intensité est environ 400x plus faible. Les RIOs montrent la forme caractéristique en feuille de trèfle aussi prévue en microscopie confocale polarisée [6,7,9,11] (Figs. 3(a) et 3(c)). Notons cependant que les RIO sont maintenant asymétriques, comme le montrent les Figs. 3(b), 3(d) et 3(e), qui présentent des coupes $x-y$ et $x-z$ à divers plans en profondeur et latéralement.

1. Introduction

In classical and even confocal microscopy [1,2], a trade-off between resolution and working distance must always be made. Long working distance objectives have a low numerical aperture, and therefore a low resolution, especially along the optical axis. High numerical aperture objectives permit a high resolution, but at the price of a usually very short working distance.

Theta microscopy has been proposed as an effective solution to combine high resolution with long working distances. Theta microscopy therefore provides the unique feature of allowing the study of large biological sample while keeping a good resolution.

In previous work, the Point Spread Function of theta microscopy was calculated using an isotropic emission model, with unpolarized excitation. However, fluorescence is known to be polarized. As a consequence, dipole emission describes better the fluorescence process.

We propose a comprehensive treatment of polarized fluorescence microscopy based on the electromagnetic theory of high numerical aperture objective, taking into account dipole emission by the fluorescent dye.

2. Polarized fluorescence theta microscopy

The idea of theta microscopy is to diminish the size of the Point Spread Function by using two microscope objectives with crossed optical axes [3]. Doing so, the lower resolution along the optical axis of the detection objective is compensated by the fact that this axis corresponds to a lateral axis for the illumination objective. Fig. 1 describes the setup considered. Objective 1 is used for fluorescence excitation, and objective 2 is for confocal detection.

This optical configuration does not allow us to use glass slides, so, the Richard and Wolf model of diffraction describes well the illumination PSF formation [1]. Considering a plane wave, linearly polarized along the x -axis, being focused by objective 1, the electric field at point P with coordinates $x = x'$, $y = -z'$,

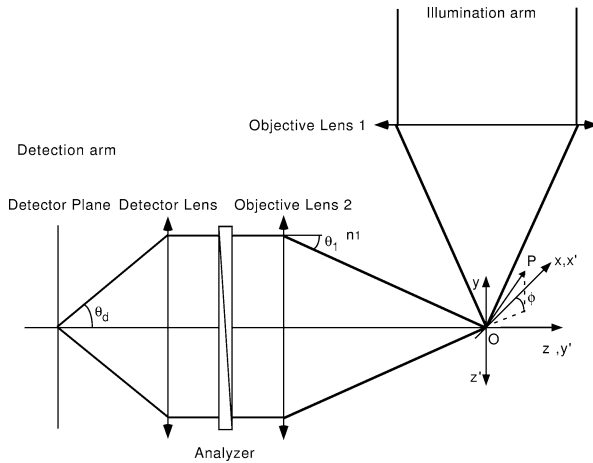


Figure 1. Sketch of a confocal theta microscope. Objective 1 is used for sample excitation. Objective 2, with optical axis at 90° with respect to objective 1, is used for detecting the fluorescence signal.

Figure 1. Schéma de principe d'un microscope confocal theta. L'objectif 1 sert à l'excitation du specimen. L'objectif 2, dont l'axe optique est à 90° de l'objectif 1, sert à la détection du signal de fluorescence.

$z = y'$ (see Fig. 1: (x, y, z) coordinates are for detection arm and (x', y', z') coordinates are for illumination arm) in the focal region is written as:

$$E_x = -i(I_0 + I_2 \cos 2\phi), \quad E_y = 2I_1 \cos \phi, \quad E_z = -i(I_2 \sin 2\phi) \quad (1)$$

with:

$$\begin{aligned} I_0 &= \int_0^\alpha a(\theta) \sin \theta (1 + \cos \theta) J_0(k \sqrt{x^2 + z^2} \sin \theta) \exp(-iky \cos \theta) d\theta, \\ I_1 &= \int_0^\alpha a(\theta) \sin^2 \theta J_1(k \sqrt{x^2 + z^2} \sin \theta) \exp(-iky \cos \theta) d\theta, \\ I_2 &= \int_0^\alpha a(\theta) \sin \theta (1 - \cos \theta) J_2(k \sqrt{x^2 + z^2} \sin \theta) \exp(-iky \cos \theta) d\theta, \end{aligned} \quad (2)$$

the Bessel function of first kind of order n . The apodization function in Eqs. (2) is given by $a(\theta) = \cos^{1/2} \theta$, ϕ the angle between the direction of observation and the x -axis (see Fig. 1), α is the objective lens aperture angle, J_n is the Bessel function of first kind of order n , and $k = k_0 \cdot n$ with n being the immersion medium refraction index.

The classical treatment of confocal or theta confocal microscopy consists in considering that the excited molecule acts as an isotropic radiator. The final Point Spread Function is simply calculated as the product of the illumination PSF by the detection PSF. For a theta setup, it is written as [3]:

$$PSF^{\text{theta}}(x, y, z) = PSF(x, y, z) \times PSF(-z, y, x) \quad (3)$$

as the difference in wavelength between illumination and detection is often neglected for simplicity. In that approach, the illumination and detection PSF are computed using the Richards and Wolf model. However, this model is for a plane wave focused into the medium, thus valid to compute the illumination PSF, but calculating the detection PSF as an illumination PSF constitutes another approximation.

Furthermore, fluorescence is known to be polarized [4,5]. A more rigorous approach therefore consists in considering a point scatterer whose far field emission is that of an electric dipole, which moment \mathbf{p} is

proportional to the illumination field [6,7]. Hence, the Cartesian components of the dipole moment are given by:

$$p_x = -i(I_0 + I_2 \cos 2\phi), \quad p_y = 2I_1 \cos \phi, \quad p_z = -i(I_2 \sin 2\phi), \quad (4)$$

the electric field in the radiation zone being given by:

$$\mathbf{E}_{dp} = -\mathbf{r} \times (\mathbf{r} \times \mathbf{p}). \quad (5)$$

The dipole electric vector is collimated by the detection objective, then passed through an analyzer and refocused onto the detector. Considering a low aperture detector lens, a quadratic detector therefore records the intensity $I = |E_d|^2$, with E_d being the Fourier transform of the scalar field [6]:

$$E_{dx} = p_x(I_0^d + I_2^d \cos 2\phi_p) + p_y I_2^d \sin 2\phi_p - 2i I_1^d p_z \cos \phi_p, \quad (6a)$$

$$E_{dy} = p_x I_2^d \sin 2\phi_p + p_y(I_0^d - I_2^d \cos 2\phi_p) - 2i I_1^d p_z \sin \phi_p \quad (6b)$$

and then one obtains the intensity PSF after the polarizer as [6]:

$$PSF(x, y, z) = |\cos^2 \gamma E_{dx} + \sin \gamma \cos \gamma E_{dy}|^2 + |\cos \gamma \sin \gamma E_{dx} + \sin^2 \gamma E_{dy}|^2 \quad (7)$$

with:

$$\begin{aligned} I_0^d &= \int_0^{\alpha_d} \sqrt{\cos \theta_1} \sin 2\theta_d J_0(k\rho \sin \theta_d)(1 + \cos \theta_1) \exp(-ikz_s \cos \theta_1) d\theta_d, \\ I_1^d &= \int_0^{\alpha_d} \sqrt{\cos \theta_1} \sin 2\theta_d J_1(k\rho \sin \theta_d) \sin \theta_1 \exp(-ik_1 z_s \cos \theta_1) d\theta_d, \\ I_2^d &= \int_0^{\alpha_d} \sqrt{\cos \theta_1} \sin 2\theta_d J_2(k\rho \sin \theta_d)(1 - \cos \theta_1) \exp(-ik_1 z_s \cos \theta_1) d\theta_d, \end{aligned} \quad (8)$$

γ being the angle between the analyzer axis and the x -axis. The angular aperture of the detector lens α_d and the coordinate angle θ_d are linked to the objective lens angular aperture α_1 and the coordinate θ_1 by the relation [6,7]:

$$\frac{n_1 \sin \alpha_1}{n_d \sin \alpha_d} = \frac{n_1 \sin \theta_1}{n_d \sin \theta_d} = \beta, \quad (9)$$

where β is the nominal magnification of the objective lens, and n_1 and n_d are the indices of refraction of the immersion medium and the image space, respectively [6,7].

3. Examples

Fig. 2 shows computed point spread functions. An Olympus Universal Plan Fluorite 40x water-immersion objective with N.A. = 0.8 is considered. This objective has a working distance of 3.3 mm and would be well suited for a theta setup, after a slight modification of the enclosure [8]. The excitation PSF is computed at $\lambda = 400$ nm and we consider emission at $\lambda = 450$ nm (corresponding to excitation and emission of Cascade Blue from Molecular Probes). The specimen is scanned through the focus. For the sake of simplicity, a point-like incoherent detector is considered [6,7]. Fig. 2(a) shows the PSF computed using the classical isotropic emission model, for unpolarized excitation and detection, using Eq. (3). Fig. 2(b) shows the PSF using the dipole model for x -polarized excitation and x -polarized detection. It is shown that the classical model tends to slightly overestimate the x -lateral resolution, while simultaneously slightly underestimates the y -lateral and z -longitudinal resolution. The dipole emission models predicts a more isotropic PSF, with better separation of the lateral lobes (more noticeable differences are expected if larger

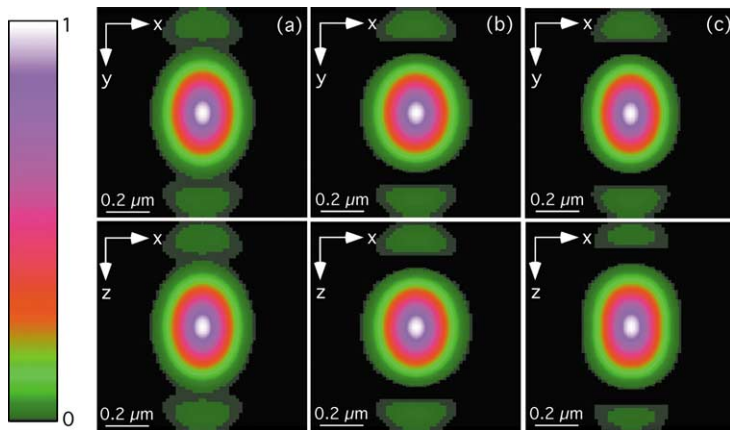


Figure 2. Point Spread Functions for a theta microscope using water immersion objectives with N.A. = 0.8, excitation at $\lambda = 400$ nm and detection at $\lambda = 450$ nm (Cascade Blue – Molecular Probes). (a) conventional unpolarized isotropic radiation model. (b), (c) dipole emission model. (b) x -polarized excitation, x -polarized detection. (c) z -polarized excitation, x -polarized detection.

Figure 2. Reponse Impulsionnelle Optique pour un microscope theta utilisant des objectifs à immersion à eau (N.A. = 0,8). Excitation à $\lambda = 400$ nm et détection à $\lambda = 450$ nm (Cascade Blue – Molecular Probes). (a) modèle classique d'émission isotrope non polarisée. (b), (c) modèle dipolaire. (b) excitation x -polarisée, détection x -polarisée. (c) excitation z -polarisée, détection x -polarisée.

N.A. objectives may be used [6,7,9]). The x -resolution is 220 nm, the y - and z -resolution being of 270 nm (versus 210 nm and 290 nm for the isotropic emission model).

An inherent problem of polarized detection in confocal microscopy is that the detection of molecules excited by light with z -axis polarization is limited by the fact that the excitation (and therefore the available signal) is much weaker than for polarization along the x -axis or the y -axis [9,10]. Typically the signal is 100 times lower [9]. A possible approach is to use phase filters to enhance the z polarized component of the excitation and detection [10].

Theta microscopy offers another possibility: as the illumination and detection axes are crossed, the optical axis for the detection arm corresponds to a lateral axis of the illumination arm, for which the component is expected to be of much higher intensity. As shown on Fig. 1, choosing a x' - or y' -polarized illumination wave corresponds to enhancing detection for the x - or z -component, respectively. The equations giving the illumination field, therefore the dipole moment, are readily obtained from Eqs. (1), (2) by a 90° rotation around the ($z' = -y$)-axis, thus permuting the roles of the variable x and $-z$. Fig. 2(c) shows the PSF obtained for z -polarized excitation and x -polarized detection. Note that the maxima of the PSFs are the same in x -polarized or z -polarized excitation. Polarized theta microscopy may therefore constitute an interesting alternative to z -polarized confocal microscopy for large specimen [10].

Fig. 3 shows PSFs computed for crossed polars, with y -polarized detection. Not only are the shapes different, but also the relative intensities of the PSFs, the detection for crossed-polarization being typically 400 times weaker. Fig. 3(a) shows the computed PSF with x -polarized excitation and y -polarized detection (in the $z = 0$ μm and $y = 0$ μm planes, respectively). It exhibits the characteristic four-leave pattern also observed in confocal polarized microscopy [6,7,9,11], but now in both planes. The pattern is however now asymmetric along the z -axis, as can be seen on Fig. 3(b), showing $x-z$ cuts along the $y = -0.18$ μm and $y = +0.18$ μm, respectively. Fig. 3(c) shows the PSF computed for z -polarized excitation and y -polarized detection (in the $z = 0$ μm and $y = 0$ μm planes, respectively). The PSF has now a very different shape, as can be seen on Figs. 3(d) and 3(e), which show cuts along various y - and z -planes. Note that a central symmetry is conserved.

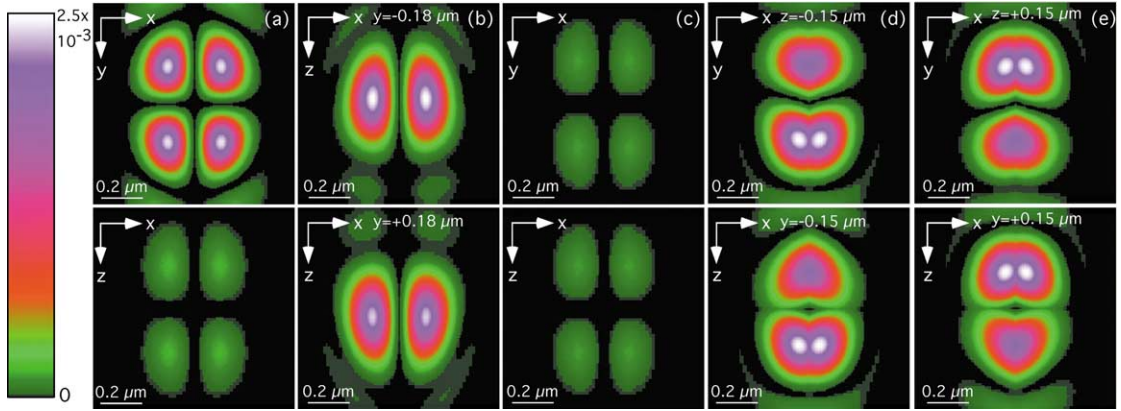


Figure 3. Same as Fig. 2, but for y -polarized detection. (a) x -polarized excitation, y -polarized detection. (b) same as (a)-bottom, but in the $y = -0.18 \mu\text{m}$ and $y = +0.18 \mu\text{m}$ plane respectively. Note the assymetry. (c) z -polarized excitation, y -polarized detection. (d), (e) same as (c) but in the $z = \pm 0.15 \mu\text{m}$ and $y = \pm 0.15 \mu\text{m}$ plane. Note the complex shape of the PSF in that case.

Figure 3. *Idem à Fig. 2, mais pour une détection y -polarisée. (a) excitation x -polarisée, détection y -polarisée. (b) identique à (a)-bas dans les plans $y = -0,18 \mu\text{m}$ et $y = +0,18 \mu\text{m}$. Notez l'assymétrie. (c) excitation z -polarisée, détection y -polarisée. (d), (e) identique à (c) mais dans les plans $z = \pm 0,15 \mu\text{m}$ et $y = \pm 0,15 \mu\text{m}$. Notez la forme complexe de la RIO dans ce cas.*

To favor the y -polarized component, one could either symetrize the detection and illumination arms, or use a second illumination objective, placed perpendicularly to the theta setup (along the x -axis), in a configuration similar to Multiple Objective Microscopy [12] or Multiple Imaging Axis Microscopy [13].

4. Conclusion

We have given a rigorous electromagnetic treatment of polarized confocal theta microscopy, using the dipole emission model to describe the fluorescence process. Formulas to compute Point Spread Functions for this type of microscopy are given as well as typical examples of PSF. The dipole emission model predicts a slightly more isotropic resolution than the isotropic emission one. The main advantage is the possibility of using strongly z -polarized excitation. Taking into account polarization properties of the fluorescence emission may permit to obtain additional information about the distribution and orientation of the dipoles in a large specimen with a good spatial resolution.

Acknowledgements. This work was made possible with the financial support of the New Energy and Industrial Technology Development Organization (NEDO) of Japan under an Industrial Technology Research Grant Program.

References

- [1] B. Richards, E. Wolf, Proc. Roy. Soc. London Ser. A 253 (1959) 349.
- [2] M. Minsky, Scanning 10 (1988) 128.
- [3] E.H.K. Stelzer, S. Lindek, Opt. Commun. 111 (1994) 536.
- [4] F. Perrin, Ann. Phys. (Paris) 12 (1929) 169.
- [5] P. Soleillet, Ann. Phys. (Paris) 12 (1929) 23.
- [6] P. Török, P.D. Higdon, T. Wilson, Opt. Commun. 148 (1998) 12.
- [7] P. Török, P.D. Higdon, T. Wilson, J. Mod. Opt. 45 (1998) 1681.
- [8] Olympus France, private communication.
- [9] C.J.R Sheppard, P. Török, Bioimaging 5 (1997) 205.
- [10] N. Huse, A. Schönle, S.W. Hell, J. Biomed. Opt. 6 (2001) 480.
- [11] T. Wilson, R. Juskaitis, P. Higdon, Opt. Commun. 141 (1997) 298.
- [12] O. Haeberlé, C. Xu, A. Dieterlen, S. Jacquy, C. R. Acad. Sci. Paris, Série IV 2 (2001) 1509.
- [13] E.H.K. Stelzer, J. Swoger, J. Huisken, Multiple imaging axis microscopie (MIAM), in: Technical Digest of Focus on Microscopy 2002, Kaohsiung, 2002, p. 58.